HHS Public Access

Author manuscript

J Immunol. Author manuscript; available in PMC 2015 April 02.

Published in final edited form as:

J Immunol. 2014 May 15; 192(10): 4859–4866. doi:10.4049/jimmunol.1301155.

SHP2 Phosphatase Promotes Mast Cell Chemotaxis toward Stem Cell Factor via Enhancing Activation of the Lyn/Vav/Rac Signaling Axis

Namit Sharma[*], **Stephanie Everingham**[*], **Baskar Ramdas**[†,‡], **Reuben Kapur**[†,‡], and **Andrew W. B. Craig**[*]

[*]Division of Cancer Biology and Genetics, Department of Biomedical and Molecular Sciences, Queen's University, Queen's Cancer Research Institute, Kingston, Ontario K7L 3N6, Canada

[†]Department of Pediatrics, Herman B. Wells Center for Pediatric Research, Indianapolis, IN 46202

[‡]Department of Biochemistry & Molecular Biology, Indiana University School of Medicine, Indianapolis, IN 46202

Abstract

SHP2 protein–tyrosine phosphatase (encoded by Ptpn11) positively regulates KIT (CD117) signaling in mast cells and is required for mast cell survival and homeostasis in mice. In this study, we uncover a role of SHP2 in promoting chemotaxis of mast cells toward stem cell factor (SCF), the ligand for KIT receptor. Using an inducible SHP2 knockout (KO) bone marrow–derived mast cell (BMMC) model, we observed defects in SCF-induced cell spreading, polarization, and chemotaxis. To address the mechanisms involved, we tested whether SHP2 promotes activation of Lyn kinase that was previously shown to promote mast cell chemotaxis. In SHP2 KO BMMCs, SCF-induced phosphorylation of the inhibitory C-terminal residue (pY507) was elevated compared with control cells, and phosphorylation of activation loop (pY396) was diminished. Because Lyn also was detected by substrate trapping assays, these results are consistent with SHP2 activating Lyn directly by dephosphorylation of pY507. Further analyses revealed a SHP2- and Lyn-dependent pathway leading to phosphorylation of Vav1, Rac activation, and F-actin polymerization in SCF-treated BMMCs. Treatment of BMMCs with a SHP2 inhibitor also led to impaired chemotaxis, consistent with SHP2 promoting SCF-induced chemotaxis of mast cells via a phosphatase-dependent mechanism. Thus, SHP2 inhibitors may be useful to limit SCF/KIT-induced mast cell recruitment to inflamed tissues or the tumor microenvironment.

Mast cells (MCs) are innate immune cells that serve as sentinels within tissues exposed to external environment and release a multitude of mediators that coordinate the immune

Address correspondence and reprint requests to: Dr. Andrew W.B. Craig, Division of Cancer Biology and Genetics, Department of Biomedical and Molecular Sciences, Queen's University, Kingston, ON K7L 3N6, Canada. andrew.craig@queensu.ca.

The online version of this article contains supplemental material.

Disclosures

The authors have no financial conflicts of interest.

response (1). However, the aberrant accumulation and activation of MCs also can result in progression of some inflammatory disorders (2). MCs also accumulate at the periphery of solid tumors and contribute to a microenvironment that facilitates tumor progression and metastasis (3). These studies imply that blocking MC recruitment mechanisms in these diseases may be an effective way to limit disease progression. Although MCs migrate toward distinct chemotactic factors depending on their degree of maturation and sensitization to Ags, the stem cell factor (SCF)/KIT signaling axis plays a key role (4). Blockade of the SCF/KIT axis has shown promise in limiting MC recruitment and mediator release leading to less disease progression (5, 6).

KIT receptor is a receptor tyrosine kinase that promotes crucial MC functions, including differentiation, survival, proliferation, migration, and homeostasis (7). KIT also promotes homing of MC progenitors to target organs and the differentiation and survival of mature MCs within connective tissues. Overexpression of SCF and KIT receptor and elevated MCs were detected in the airways of asthma patients (8, 9), and blockade of SCF/KIT improved airway function (10, 11). KIT receptor blockade also has improved symptoms in allergic rhinitis, scleroderma, and rheumatoid arthritis (5). MCs also are recruited to a variety of solid tumors that secrete SCF (12–14), and this triggers MC release of mediators enhancing tissue remodeling and immunosuppression. These studies suggest that inhibitors of MC chemotaxis and mediator release may improve outcomes in these diseases with MC involvement.

Src homology region 2 domain-containing phosphatase 2 (SHP2) is a protein tyrosine phosphatase (PTP) that signals downstream of KIT in multiple cell types. Recently, SHP2 was implicated in KIT signaling pathways leading to survival and homeostasis of hematopoietic stem cells (HSCs) (15, 16). In addition, SHP2 also promotes survival of MCs via enhancing KIT signaling to ERK and downregulation of Bim (17). The KIT juxtamembrane (pY567/pY569) pathway promotes recruitment and activation of SHP2 via the Shc/Grb2/Gab2 adaptor proteins, and downstream signaling to the Ras and Rac-JNK pathways (18). KIT pY567/pY569 signaling has also been implicated in regulation of cell migration through enhancing Lyn kinase activation and calcium mobilization (19). However, the contribution of SHP2 to Lyn activation and chemotaxis of MCs has not been previously reported. We previously reported that SHP2 knockout (KO) bone marrow–derived mast cells (BMMCs) fail to repopulate mast cell–deficient mice (17), and these defects were more pronounced than the effects on MC survival in vitro. This led us to speculate that SHP2 coordinates other aspects of MC homeostasis in vivo, including mast cell adhesion and motility.

In this study, we identify a SHP2-dependent pathway promoting MC chemotaxis toward SCF using both an inducible SHP2 KO BMMC model (17, 20) and stable silencing of SHP2 in Baf/3-KIT cells. In both systems, this corresponded to defects in SCF/KIT-induced activation of Lyn. Downstream signaling from Lyn also was impaired, including reduced phosphorylation of the Rac GEF Vav1 and less active Rac^{GTP} at the plasma membrane of SHP2 KO BMMCs. This correlated with reduced F-actin polymerization upon SCF treatment of SHP2 KO cells. Because SHP2 inhibitor treatment of BMMCs caused similar defects in Lyn activation and chemotaxis of BMMCs, this raises the possibility of using

SHP2 inhibitors to limit aberrant accumulation of MCs in disease conditions such as inflammatory disorders and cancers that secrete SCF.

Materials and Methods

Mice

Transgenic Tg^{CreER}:$Shp2^{fl/fl}$ and $Shp2^{fl/fl}$ mice (C57BL/6 background) were described previously (1). All animals were housed and bred at Queen's University Animal Care Services, and all procedures were approved by the Queen's University Animal Care committee in accordance with Canadian Council on Animal Care guidelines. $Lyn^{-/-}$ mice (C57BL/6 background) (21) were maintained under specific pathogen-free conditions at the Indiana University Laboratory Animal Research Center (Indianapolis, IN), and the study was approved by the Institutional Animal Care and Use Committee of the Indiana University School of Medicine.

Reagents

The following primary Abs were used: mouse anti-Rac1 (Millipore), mouse anti-active Rac (NewEast Biosciences), rabbit anti–pY507-Lyn (Epitomics), rabbit anti–pY416-Src (Cell Signaling Technology; cross reacts with pY396-Lyn), rabbit anti–pY527-Src (Cell Signaling Technology; cross reacts with pY528-Fyn), anti-Fyn (Santa Cruz Biotechnology), rabbit anti-Vav1 (C-14; Santa Cruz Biotechnology), rabbit anti-ERK (Santa Cruz Biotechnology), mouse anti–β-actin (Santa Cruz Biotechnology), anti-tubulin (Sigma-Aldrich), mouse anti-pY99 (Santa Cruz Biotechnology), rabbit anti-SHP2 (Santa Cruz Biotechnology), and rabbit anti-Lyn (Santa Cruz Biotechnology). Secondary Abs were Alexa Fluor 488–conjugated goat anti-mouse IgG (Invitrogen) and Alexa Fluor 568–conjugated goat anti-rabbit IgG (Invitrogen). Other reagents included the following: recombinant murine SCF (PeproTech), CellTracker Green and CellTracker Orange (Invitrogen), bovine fibronectin (Roche Diagnostics), and tetramethylrhodamine isothiocyanate (TRITC)– and Alexa Flour 488–conjugated phalloidin (Invitrogen).

BMMC cultures

BMMC cultures were established from femoral bone marrow cells as described previously (20). In the presence of IL-3–conditioned media, nonadherent cells at 4–6 wk were mature MCs based on high expression of KIT and FcεRIα tested by flow cytometry. Mature BMMCs from $Shp2^{fl/fl}$ and Tg^{CreER}:$Shp2^{fl/fl}$ mice were treated with 4-hydroxytamoxifen (4TM; Sigma-Aldrich) for 3 d to obtain wild-type (WT) and KO cultures, respectively. The extent of SHP2 inactivation was determined by SHP2 immunoblot and PCR analysis of genomic DNA, as described previously (17). $Lyn^{-/-}$ BMMCs were generated from $Lyn^{-/-}$ mice as described above and tested for maturity (>95% KIT^{+}/FcεRIα^{+}) prior to experiments (WT C57BL/6 mice served as $Lyn^{+/+}$ control).

SCF treatment and immunoblotting

For SCF stimulation, BMMCs (5×10^6/sample) were starved of IL-3 for 6 h, washed twice in Tyrode's buffer (10 mM HEPES [pH 7.5], 130 mM NaCl, 5 mM KCl, 1.4 mM $CaCl_2$,1 mM $MgCl_2$, 5.6 nM glucose, and 0.1% BSA), and stimulated with or without SCF (50

ng/ml; PeproTech) for 5 or 15 min at 37°C. In case of II-B08 treatment, BMMCs were grown in the presence of IL-3/SCF for 3 wk and then treated with either DMSO or different concentrations of II-B08 (10–50 μM) for 1 h at 37°C. Lysates were prepared as described previously (20). Immunoprecipitations (IPs) were performed with rabbit anti-Vav IgG overnight at 4°C, recovered using GammaBind Sepharose (GE Healthcare), and washed prior to immunoblotting (IB) with indicated Abs. Signals were revealed by using appropriate HRP-conjugated secondary Abs and ECL reagents (Pierce, Thermo Scientific).

Chemotaxis assays

Transwell filters (BD Biosciences) were used to assess chemotaxis of BMMC (3 μm pore) or Baf3-KIT (8 μm pore) cells as reported previously (22). Briefly, filters were coated with fibronectin (20 μg/ml) overnight at 4°C, and cells starved of IL-3 (4×10^5/well) were plated in the upper chamber and allowed to migrate toward media containing SCF (25 ng/ml) in the lower chamber for 4 h at 37°C. Nonmigrating cells in the upper chamber were removed with a cotton swab prior to fixation of migrating cells with 4% paraformaldehyde and staining with DAPI (300 nM). Filters were imaged using an epifluorescence microscope, and images were analyzed using ImageJ (National Institutes of Health) to score migrating cells. In case of Baf/3-KIT cells, migrating cells within the lower chamber were scored using an automated cell counter. Agarose drop chemotaxis assays using SCF-embedded agarose was described recently (13). Briefly, SCF (30 ng/ml) was embedded in a drop containing 0.5% low-melt agarose and allowed to solidify on dried coverslips previously coated with fibronectin (20 μg/ml) and stabilized at 4°C for 15 min. Starved BMMCs (4×10^6; WT or KO) were treated with either DMSO or different doses of II-B08 (10–20 μM) and slowly added to each for 18–24 h at 37°C. Subsequently, agarose drops were carefully removed, and cells on the coverslip were fixed with cold 4% paraformaldehyde, prior to staining with DAPI to visualize cell nuclei. To quantify migration of cells under the agarose drop, epifluorescence micrographs were acquired using DAPI staining and analyzed using ImageJ software. The viability of cells treated with II-B08 or vehicle was assessed using alamar blue assays, as described previously (17).

For live cell imaging, WT and KO BMMCs were starved of cytokines, stained with CellTracker Orange and Green (Invitrogen; 5 μM), respectively, and mixed at a 1:1 ratio (1×10^6 total cells). Cells were seeded on coverslips and allowed to migrate for 18 h in a climate-controlled chamber mounted on a WaveFX spinning disc confocal microscope (×10 objective, 21 z-axis slices; Quorum Technologies). Images were acquired every 2 min for multiple fields spanning the edge of the agarose drop. Metamorph software was used to compile overlay images and videos, whereas the calculation of migration parameters (distance, velocity) was performed by tracking individual cells using ImageJ software.

Immunofluorescence

For spreading and polarization assays, starved WT and KO BMMCs were plated on fibronectin (20 μg/ml)-coated coverslips in SCF (25 ng/ml) containing media for 45 min. Immunofluorescence staining was performed after fixation in cold 4% paraformaldehyde, permeabilization in PBS/0.2% Triton X-100, and incubated with anti-active Rac1 Ab (1:75) and anti-Lyn Ab (1:50) overnight at 4°C. Active-Rac1, Lyn, and F-actin were detected using

TRITC–phalloidin (1:200), Alexa Fluor 488–conjugated goat anti-mouse IgG, and Alexa Flour 568–conjugated goat anti-rabbit IgG (1:200) or TRITC–phalloidin alone for 1 h at room temperature. After washing three times with PBS, cells on the coverslip were stained with DAPI (300 nM) for 10 min at room temperature, followed by mounting coverslips on glass slides. Confocal micrographs were acquired using a Leica TCS SP2 Multi Photon confocal microscope (HCX PL APO DIC ×63/1.32 Oil CS objective). The quantification of cell spreading and polarization was acquired using ImageJ software. Total internal reflective fluorescence (TIRF) micrograph was acquired using WaveFX spinning disc confocal microscope equipped with TIRF module (Spectral Applied Research). Colocalization analysis of active-Rac1 and F-actin channels was performed on overlayed images (n = 20) to calculate Mander's coefficient using colocalization plug-in for ImageJ software.

F-actin polymerization assays

Total F-actin was measured in BMMCs treated with or without SCF as recently described (23). Briefly, WT and KO BMMCs were starved of IL-3 for 6 h, resuspended at 10^6/ml in Tyrode's buffer [10 mM Hepes pH 7.4, 130 mM NaCl, 5 mM KCl, 1.4 mM $CaCl_2$, 1 mM $MgCl_2$, 5.6 mM glucose, 0.1% BSA], and treated with SCF (100 ng/ml) for 0–30 min. Aliquots (0.5 ml) were removed at indicated times and fixed in cold 4% paraformaldehyde/5 mM EGTA/5 mM EDTA and permeabilized in PBS/0.1% saponin/2% BSA. Cells were stained with 10 nM AlexaFluor-488-conjugated phalloidin for 1 h, rinsed, and analyzed by flow cytometry.

Substrate trapping

Baf/3-KIT SHP2 KD2 cells (2×10^8 cells) were stimulated with SCF (50 ng/ml) for 5 min and lysed with substrate trapping buffer (20 mM Tris [pH 7.5], 100 mM NaCl, 1% Triton X-100, 10% glycerol, 5 mM iodoacetic acid, 1 mM vanadate, 10 μg aprotinin/ml, 10 μg leupeptin/ml, and 100 μM phenylmethyl sulfonyl fluoride) to obtain lysates. Excess iodoacetic acid was denatured with 10 mM DTT for 15 min at 4°C, prior to incubation with GST or a GST fusion to human SHP2 PTP domain [with D425A/Q506A [D/A:Q/A] substrate trapping mutations (24)] that were prebound to glutathione Sepharose 4B beads. After incubation overnight at 4°C, beads were washed three times with ice-cold substrate trapping buffer supplemented with 1 mM EDTA and denatured with SDS-PAGE sample buffer and analyzed by IB with indicated Abs.

Baf/3-KIT cells and SHP2 silencing

Baf3-KIT cells were previously reported (19) and were grown in RPMI 1640/10% FBS/2% (v/v) IL-3–conditioned media. Baf3-KIT cells were transduced with pGIPZ-based lentiviruses expressing nontargeting (NT) or mouse SHP2–specific short hairpin RNAs (shRNAs; Invitrogen). Lentiviral packaging, transduction, and titer evaluation was accomplished as described previously (2). Single clones of each transduced shRNAs were identified and isolated based on sorting of GFP-positive cells by FACS. The most effective shRNAs (shRNA1: clone A9 (V3LMM_430009), mature antisense, 5′-TTATCTGTGGTCTCAGCCA-3′; shRNA2: clone C2 (V2LMM_782273), mature

antisense, 5′-ATATTGGTATATTCATGTC-3′) were determined following immunoblot analysis and correspond to KD1 and KD2 cell lines, respectively.

Statistical analyses

Differences between control and SHP2 KO or KD cells were analyzed using paired Student *t* test, and statistically significant differences ($p < 0.05$) are indicated within figures. All assays were conducted with experimental and assay replicates included.

Results

SHP2 promotes MC spreading, polarization, and chemotaxis toward SCF

SCF/KIT signaling leads to increased adhesion, spreading, polarization, and motility of MCs (25–27). To test the role of SHP2 in these processes, we generated BMMCs from $shp2^{fl/fl}$ and $Tg^{Cre\text{-}ER}$: $shp2^{fl/fl}$ mice, and upon reaching maturity ($FceRI^{+}/KIT^{+}$ > 95%), we treated with 4-TM (200 nM) for 3 d to generate WT and KO MCs, as described previously (17, 20). Genomic DNA from WT and KO BMMCs was subjected to PCR analysis of floxed and null alleles of Shp2. As expected, null alleles were generated only in KO BMMCs (Fig. 1A), and this led to reduced levels of SHP2 protein in KO compared with WT BMMCs (Fig. 1B). We and others have previously demonstrated defects in KIT signaling to cell proliferation and survival pathways in SHP2 KO BMMCs (17, 28). However, the potential role of SHP2 in regulating cytoskeletal reorganization and MC motility has not been reported. To assess this, WT and KO BMMCs were allowed to attach and spread on fibronectin-coated coverslips in the presence of SCF. At early times (15 min), no differences in BMMC attachment were observed between genotypes (data not shown). However, at later times (45 min), the majority of WT BMMCs had undergone cell spreading, and this was less frequently observed in KO BMMCs (Fig. 1C). Quantification of these cell spreading assays revealed a significant difference in WT BMMCs (69 ± 3.7%) compared with KO BMMCs (47 ± 7.4%; Fig. 1D). Similar defects in percentage of polarized MCs were observed in KO BMMCs compared with WT BMMCs (Fig. 1E). Taken together, these results implicate SHP2 in promoting spreading and polarization of MCs induced by SCF/KIT signaling.

Next, we tested whether SHP2 also promotes chemotaxis response to SCF in BMMCs. WT and KO BMMCs were placed in Transwell chambers for chemotaxis toward SCF as described above. In these assays, we observed 54% reduction in migrating KO BMMCs compared with WT (Fig. 2A). Similar defects were observed in Baf3/KIT cells with stable SHP2 knockdown (KD) compared with an NT shRNA (Supplemental Fig. 1A, 1B). To extend on these findings, we analyzed WT and KO BMMC chemotaxis toward SCF-embedded agarose drops by time-lapse microscopy, as described previously (13). To simultaneously analyze WT and KO BMMCs under identical conditions, WT and KO cells were stained with CellTracker Orange (WT) or Green (KO) and mixed briefly prior to addition to wells containing fibronectin-coated coverslips containing SCF-embedded agarose drops (Fig. 2B). Both WT and KO BMMCs adhered to the coverslips surrounding the agarose drops within 30 min, and then, coverslips were mounted in imaging chambers (37°C, 5% CO_2), and live cell imaging was performed by confocal microscopy for up to 16 h. We observed increased numbers of WT BMMCs that migrated under the agarose drop

compared with KO BMMCs (Fig. 2C, see arrows; Supplemental Video 1). Quantification of individual WT and KO cells from multiple fields of view revealed significant defects in both total migration distance and cell velocity for SHP2 KO compared with WT BMMCs (Fig. 2D, 2E). Overall, these results identify SHP2 as a positive regulator of KIT-driven chemotaxis of MCs.

Lyn is a substrate of SHP2 downstream of KIT

Previously, KIT juxtamembrane signaling to Src family kinases (SFK) including Lyn and Fyn kinases have been shown to enhance chemotaxis of cells toward SCF (19, 25, 29). To test whether SHP2 regulates KIT signaling to Lyn and Fyn, we compared levels of inhibitory phosphorylation sites in Lyn (pY507) and Fyn (pY528) kinases in NT and SHP2 KD2 cells treated with SCF. As expected, SCF treatment of Baf/3-KIT NT control cells led to rapid dephosphorylation of Lyn at Y507, consistent with Lyn activation downstream of KIT (Supplemental Fig. 1C). In contrast, SCF-treated SHP2 KD cells had 2- to 3-fold higher levels of pY507-Lyn compared with NT controls (Supplemental Fig. 1C). We also tested SCF/KIT signaling to Lyn is affected in SHP2 KO BMMCs. SCF stimulation of WT BMMCs led to dephosphorylation of Lyn Y507 within 5 min and returned to baseline levels at 15 min (Fig. 3A, 3B). However, significantly higher levels of pY507-Lyn were observed in SHP2 KO BMMCs compared with WT (Fig. 3A, 3B). In addition, the SCF-induced increase in activation loop phosphorylation of Lyn (pY396) observed in WT BMMCs was not detected in SHP2 KO BMMCs (Fig. 3A, 3C). Taken together, these results suggest that SHP2 is required for Lyn activation downstream of KIT.

In parallel studies of Fyn, we observed no differences in SCF/KIT-induced dephosphorylation of Y528 in Fyn between NT and SHP2 KD2 cells (Supplemental Fig. 1C, *lower panels*). The lack of involvement of SHP2 in Fyn activation is consistent with a recent study implicating PTPα in activation of Fyn, but not Lyn, in BMMCs treated with SCF (30).

Although SHP2 is known to promote SFK activation indirectly via dephosphorylating recruitment sites for Csk in a variety of growth factor pathways (31), a recent study identified pY507-Lyn as a direct substrate of SHP2 in the G-CSF receptor pathway (32). To test whether Lyn is a direct substrate of SHP2 in the SCF/KIT pathway, substrate trapping assays were conducted on lysates prepared from SCF-treated SHP2 KD Baf/3-KIT cells, which are expected to have increased phosphorylation levels of SHP2 substrates. The PTP domain of SHP2 with substrate trapping mutations (D/A:Q/A) (24, 33) was expressed and purified as a GST fusion (GST-PTP$^{D/A:Q/A}$) and used along with GST as a negative control to conduct pull-down assays in the absence (mock) and presence of SCF-treated cell lysates (+ lysate). Both pY507-Lyn and total Lyn were recovered at much higher levels with GST-PTP$^{D/A:Q/A}$ compared with GST alone (Fig. 3D). Other proteins including the previously identified SHP2 substrate p190RhoGAP were not recovered in these assays, likely because of lack of phosphorylation in SCF-treated cells (Fig. 3D). Taken together, these results identify SHP2 as a key PTP involved in Lyn activation within the SCF/KIT pathway, and this likely contributes to defects in chemotaxis of SHP2 KO BMMCs.

SHP2 and Lyn promote KIT signaling to Vav1 in BMMCs

Vav1 is a highly expressed Rac GEF that is recruited to activated KIT and its GEF activity is enhanced via tyrosine phosphorylation in an SFK-dependent manner (30, 34, 35). To test whether Lyn activation defects observed in SHP2 KO BMMCs impair downstream signaling to Vav1, we compared Vav1 pY in WT and KO BMMCs treated with or without SCF. As expected, SCF treatment of WT BMMCs led to increased Vav1 pY, however, this response was blunted in SHP2 KO BMMCs (Fig. 4A, 4B). To test whether SHP2 regulates Vav1 pY via Lyn activation, we generated $Lyn^{+/+}$ and $Lyn^{-/-}$ BMMCs (Fig. 4C) and performed similar analysis of Vav1 pY upon SCF treatment. We observed a marked reduction in SCF-induced Vav1 pY in the absence of Lyn (Fig. 4D). Taken together, these results implicating SHP2 and Lyn in promoting Vav1 pY may contribute to activation of Rho family GTPases involved in MC chemotaxis.

SHP2 promotes Rac1 activation and F-actin polymerization via SCF/KIT axis

To further define the potential defects associated with reduced phosphorylation of Vav in KO BMMCs, we measured the levels of active Rac at the plasma membrane of actively migrating BMMCs. WT and KO BMMCs were stimulated with SCF to induce adhesion to fibronectin-coated coverslips, which promotes translocation of active Rac to membranes (36) and the appearance of polarized and motile cells (25). An Ab specific for active conformation of Rac1 ($Rac1^{GTP}$) was used for immunofluorescence staining, and the membrane pool was visualized using TIRF microscopy. In WT BMMCs, active Rac was readily detected at the cell periphery and was colocalized with Lyn and F-actin (Fig. 5A). In contrast, KO BMMCs showed less active Rac at the cell periphery and less colocalization of $Rac1^{GTP}$ with F-actin (Fig. 5A, 5B). Because Rac activation leads to increased F-actin branching and poly-merization at the leading edge of motile cells (37), we tested whether SHP2 KO BMMCs have defects in SCF-induced F-actin polymerization. Using a flow cytometry-based assay of SCF-induced changes in F-actin that was previously reported (38), WT and KO BMMCs were treated with SCF (0–30 min) prior to permeabilization, staining with phalloidin, and analysis by flow cytometry. As expected, SCF treatment of WT BMMCs led to a rapid increase in total F-actin levels compared with untreated cells (Fig. 5C). In contrast, KO BMMCs showed a net loss of F-actin at early times (2–10 min), prior to net gains in F-actin at later times that approached the levels of WT BMMCs (Fig. 5C). This delay in SCF-induced F-actin polymerization likely contributes to cell spreading and motility defects we observed, which are consistent with SHP2 enhancing KIT signaling to a Lyn/Vav/Rac pathway in MCs.

SHP2 inhibitor limits chemotaxis of BMMCs toward SCF

To investigate whether SHP2 scaffolding function or phosphatase activity was responsible for its role in promoting BMMC chemotaxis toward SCF, we used the recently described SHP2 inhibitor II-B08 (17, 39). BMMCs were pretreated with either vehicle (DMSO) or increasing doses of II-B08 (10 or 20 μM). Lysates were subjected to IB with anti–phospho-ERK (pERK), because ERK activation is positively regulated by SHP2 downstream of KIT in BMMCs (17). Indeed, less pERK was observed in the presence of II-B08 compared with DMSO (Fig. 6A). Likewise, II-B08 treatment led to increased levels of pY507-Lyn in

BMMCs (Fig. 6A). At these doses of II-B08, only a moderate reduction in cell viability was observed in BMMCs (Fig. 6B; not statistically significant).

Next, we tested whether SHP2 inhibitor can mimic the effects of gene KO in SCF-induced chemotaxis assays. BMMCs were treated with either DMSO or II-B08 (10 or 20 μM) and analyzed using the agarose drop chemotaxis assay. We observed no effects of II-B08 treatment on the ability of BMMCs to adhere to coverslips surrounding the SCF-embedded agarose drop; however, fewer cells migrated underneath the drop in cells treated with 20 μM II-B08 (Fig. 6C, 6D). Taken together, these results implicate SHP2 phosphatase activity in promoting Lyn activation and downstream signaling pathway, which drives chemotaxis of MCs (Fig. 6E).

Discussion

SHP2 is a key mediator of SCF/KIT signaling that enhances MC proliferation and survival pathways (17, 18). Although SHP2 modulates these key facets of KIT signaling in vitro, the magnitude of these defects was unlikely to fully explain the severe defect in MC homeostasis we observed in MC-specific SHP2 KO mice (17). We hypothesized that SHP2 also may promote aspects of MC homing and motility within connective tissues. SCF is a potent chemoattractant of MCs both in vitro and in vivo, and localized SCF production leads to MC accumulation at sites of inflammation and tumorigenesis (5, 6). In this study, we report that SHP2 is a positive regulator of MC chemotaxis toward SCF using genetic and pharmacological approaches. Using both SHP2 gene silencing in Baf/3-KIT cells and SHP2 KO BMMCs, we observed reduced chemotaxis toward SCF. KIT juxtamembrane signaling to SFKs was previously implicated in chemotaxis toward SCF (19). Because SHP2 enhances SFK activation in several growth factor pathways (31), we tested its effects on Lyn and Fyn kinases that both contribute to MC chemotaxis (25, 29). In both Baf/3-KIT and BMMCs models, SHP2 was found to promote dephosphorylation of inhibitory Y507 in Lyn upon SCF treatment. In contrast, Fyn kinase dephosphorylation downstream of KIT was independent of SHP2 and is consistent with PTPα being responsible for Fyn but not Lyn activation downstream of KIT (30). Further analysis by substrate trapping identified Lyn as a direct substrate of SHP2 in SCF-treated cells. This is consistent with another recent study implicating SHP2 in dephosphorylating Lyn pY507 to promote Lyn activation downstream of G-CSF receptor (32). The coordination of SHP2 and Lyn signaling downstream of KIT (Fig. 6E) is consistent with both proteins being required for optimal chemo-taxis of MCs toward SCF (29).

Rac GTPases play key roles in SCF/KIT signaling to gene expression and cytoskeletal regulation in MCs (40). KIT signaling to Rac GEFs and GAPs leads to temporal and spatial control of a pool of active Rac (Rac^{GTP}) that signals to downstream effectors in MCs. Although a previous study identified SHP2 as a positive regulator of KIT signaling to Rac (28), the signaling mechanism remained unclear. In this study, we extend on these analyses to show that SHP2 enhances the plasma membrane pool of Rac^{GTP} in SCF-treated BMMCs undergoing cell spreading and polarization. This finding suggests that SHP2 either promotes activation of Rac GEFs or inhibition of a Rac GAPs. Previous studies implicate SFKs in promoting Rac activation and tyrosine phosphorylation of the Rac GEF Vav (25, 30, 41).

Consistent with reduced Lyn activation in SCF-treated SHP2 KO BMMCs, we also observed less Vav1 pY in these cells compared with WT BMMCs. This is consistent with a KIT/SHP2/Lyn/Vav1/Rac pathway to regulate chemotaxis of MCs (Fig. 6E). SHP2 also may regulate chemotaxis via Rho GAPs. For example, β2-chimaerin is a Rac GAP and SFK substrate implicated in breast cancer progression that would be worth testing in future studies (42). Rac effectors include key regulators of F-actin polymerization and branching, such as the PAK/Cortactin/Arp2/3 and WAVE/Scar/Arp2/3 complexes (43). Our findings that SHP2 KO BMMCs show delayed F-actin polymerization upon SCF treatment is consistent with the observed defects in signaling and Rac^{GTP} at the plasma membrane. This is expected to contribute to the defects in cell spreading and motility we observed in SHP2-deficient MCs.

A number of studies highlighted the role of KIT receptor and its downstream effector including SFKs, PI3K, and Gab2 in MC migration. In this study, we report that SHP2 promotes both the intrinsic velocity and persistence of MC chemotaxis toward SCF, as measured by live cell imaging. Importantly, these agarose drop assays allowed us to simultaneously visualize chemotaxis of WT and KO BMMCs and provided additional evidence for direct regulation of motility by SHP2. The additional testing of SHP2 inhibitor II-B08 in BMMC chemotaxis toward SCF revealed that SHP2 PTP activity is largely responsible for its promigratory role. This is consistent with SHP2 recruitment and activation to KIT-Grb2-Gab2 complexes following MC exposure to SCF (28), and this likely colocalizes active SHP2 with inhibited pool of Lyn (pY507-Lyn) at the plasma membrane. Subsequent dephosphorylation of Lyn leads to phosphorylation of downstream substrates such as Vav and Rac signaling to actin regulatory proteins that promote cytoskeletal reorganization and motility. It is certainly possible that SHP2 silencing or KO also impairs signaling that requires SHP2 scaffolding functions, as reported in for signaling by LEOPARD syndrome mutations in SHP2 (44, 45). Future studies will be required to directly test the relative effects of genetic and pharmacological blockade of SHP2 function in MCs in vitro and in vivo. Of particular interest would be testing SHP2 inhibitors in cancer models, whereby SHP2 inhibition within both tumor cells and stromal MCs might lead to reduced tumor progression. Recently, both genetic and pharmacological approaches to inhibit SHP2 resulted in reduced KIT^{D814V}-driven myeloproliferative disease in mice and identified SHP2 as a druggable target (46). Future studies also will be required to test the effects of SHP2 inhibitors on recruitment of MCs to the tumor microenvironment, and whether this limits tumor progression to meta-static disease. SHP2 inhibitors also may reduce accumulation of MCs at sites of allergic inflammation and could be tested in these disease models as well.

Supplementary Material

Refer to Web version on PubMed Central for supplementary material.

Acknowledgments

This work was supported by operating grants from the Canadian Institutes for Health Research (MOP82882) (to A.W.B.C.).

We thank members of the Craig laboratory for helpful discussions, Dr. Zhong-Yin Zhang for providing II-B08, and the staff of the Queen's Cytometry and Imaging facility for assistance.

Abbreviations used in this article

BMMC	bone marrow–derived mast cell
DRM	detergent-resistant membrane
HSC	hematopoietic stem cell
IB	immunoblotting
IP	immunoprecipitation
KD	knockdown
KO	knockout
MC	mast cell
NT	non-targeting
PTP	protein-tyrosine phosphatase
SCF	stem cell factor
SFK	Src family kinase
SHP2	SH2 domain-containing phosphatase-2
shRNA	short hairpin RNA
TIRF	total internal reflective fluorescence
4TM	4-hydroxytamoxifen
TRITC	tetramethylrhodamine isothiocyanate
WT	wild-type

References

1. Tsai M, Grimbaldeston M, Galli SJ. Mast cells and immunoregulation/immunomodulation. Adv Exp Med Biol. 2011; 716:186–211. [PubMed: 21713658]
2. Collington SJ, Williams TJ, Weller CL. Mechanisms underlying the localisation of mast cells in tissues. Trends Immunol. 2011; 32:478–485. [PubMed: 21917522]
3. Ribatti D, Crivellato E. Mast cells, angiogenesis and cancer. Adv Exp Med Biol. 2011; 716:270–288. [PubMed: 21713661]
4. Halova I, Draberova L, Draber P. Mast cell chemotaxis - chemo-attractants and signaling pathways. Front Immunol. 2012; 3:119. [PubMed: 22654878]
5. Reber L, Da Silva CA, Frossard N. Stem cell factor and its receptor c-Kit as targets for inflammatory diseases. Eur J Pharmacol. 2006; 533:327–340. [PubMed: 16483568]
6. Maltby S, Khazaie K, McNagny KM. Mast cells in tumor growth: angiogenesis, tissue remodelling and immune-modulation. Biochim Biophys Acta. 2009; 1796:19–26. [PubMed: 19233249]
7. Lennartsson J, Rönnstrand L. Stem cell factor receptor/c-Kit: from basic science to clinical implications. Physiol Rev. 2012; 92:1619–1649. [PubMed: 23073628]
8. Da Silva CA, Blay F, Israel-Biet D, Laval AM, Glasser N, Pauli G, Frossard N. Effect of glucocorticoids on stem cell factor expression in human asthmatic bronchi. Clin Exp Allergy. 2006; 36:317–324. [PubMed: 16499642]

9. Al-Muhsen SZ, Shablovsky G, Olivenstein R, Mazer B, Hamid Q. The expression of stem cell factor and c-kit receptor in human asthmatic airways. Clin Exp Allergy. 2004; 34:911–916. [PubMed: 15196279]
10. Campbell E, Hogaboam C, Lincoln P, Lukacs NW. Stem cell factor-induced airway hyperreactivity in allergic and normal mice. Am J Pathol. 1999; 154:1259–1265. [PubMed: 10233863]
11. Olsson N, Rak S, Nilsson G. Demonstration of mast cell chemotactic activity in bronchoalveolar lavage fluid collected from asthmatic patients before and during pollen season. J Allergy Clin Immunol. 2000; 105:455–461. [PubMed: 10719293]
12. Huang B, Lei Z, Zhang GM, Li D, Song C, Li B, Liu Y, Yuan Y, Unkeless J, Xiong H, Feng ZH. SCF-mediated mast cell infiltration and activation exacerbate the inflammation and immunosuppression in tumor microenvironment. Blood. 2008; 112:1269–1279. [PubMed: 18524989]
13. Kwok E, Everingham S, Zhang S, Greer PA, Allingham JS, Craig AW. FES kinase promotes mast cell recruitment to mammary tumors via the stem cell factor/KIT receptor signaling axis. Mol Cancer Res. 2012; 10:881–891. [PubMed: 22589410]
14. Théou-Anton N, Tabone S, Brouty-Boyé D, Saffroy R, Ronnstrand L, Lemoine A, Emile JF. Co expression of SCF and KIT in gastrointestinal stromal tumours (GISTs) suggests an autocrine/paracrine mechanism. Br J Cancer. 2006; 94:1180–1185. [PubMed: 16570044]
15. Zhu HH, Ji K, Alderson N, He Z, Li S, Liu W, Zhang DE, Li L, Feng GS. Kit-Shp2-Kit signaling acts to maintain a functional hematopoietic stem and progenitor cell pool. Blood. 2011; 117:5350–5361. [PubMed: 21450902]
16. Chan G, Cheung LS, Yang W, Milyavsky M, Sanders AD, Gu S, Hong WX, Liu AX, Wang X, Barbara M, et al. Essential role for Ptpn11 in survival of hematopoietic stem and progenitor cells. Blood. 2011; 117:4253–4261. [PubMed: 21398220]
17. Sharma N, Kumar V, Everingham S, Mali RS, Kapur R, Zeng LF, Zhang ZY, Feng GS, Hartmann K, Roers A, Craig AW. SH2 domain-containing phosphatase 2 is a critical regulator of connective tissue mast cell survival and homeostasis in mice. Mol Cell Biol. 2012; 32:2653–2663. [PubMed: 22566685]
18. Yu M, Lowell CA, Neel BG, Gu H. Scaffolding adapter Grb2-associated binder 2 requires Syk to transmit signals from FcepsilonRI. J Immunol. 2006; 176:2421–2429. [PubMed: 16456001]
19. Ueda S, Mizuki M, Ikeda H, Tsujimura T, Matsumura I, Nakano K, Daino H, Honda Zi Z, Sonoyama J, Shibayama H, et al. Critical roles of c-Kit tyrosine residues 567 and 719 in stem cell factor-induced chemotaxis: contribution of src family kinase and PI3-kinase on calcium mobilization and cell migration. Blood. 2002; 99:3342–3349. [PubMed: 11964302]
20. McPherson VA, Sharma N, Everingham S, Smith J, Zhu HH, Feng GS, Craig AW. SH2 domain-containing phosphatase-2 protein-tyrosine phosphatase promotes FcεRI-induced activation of Fyn and Erk pathways leading to TNF α release from bone marrow-derived mast cells. J Immunol. 2009; 183:4940–4947. [PubMed: 19786542]
21. Ma P, Vemula S, Munugalavadla V, Chen J, Sims E, Borneo J, Kondo T, Ramdas B, Mali RS, Li S, et al. Balanced interactions between Lyn, the p85α regulatory subunit of class I(A) phosphatidylinositol-3-kinase, and SHIP are essential for mast cell growth and maturation. Mol Cell Biol. 2011; 31:4052–4062. [PubMed: 21791602]
22. Craig AW, Greer PA. Fer kinase is required for sustained p38 kinase activation and maximal chemotaxis of activated mast cells. Mol Cell Biol. 2002; 22:6363–6374. [PubMed: 12192036]
23. Ito T, Smrž D, Jung MY, Bandara G, Desai A, Smržzová S, Kuehn HS, Beaven MA, Metcalfe DD, Gilfillan AM. Stem cell factor programs the mast cell activation phenotype. J Immunol. 2012; 188:5428–5437. [PubMed: 22529299]
24. Kontaridis MI, Eminaga S, Fornaro M, Zito CI, Sordella R, Settleman J, Bennett AM. SHP-2 positively regulates myogenesis by coupling to the Rho GTPase signaling pathway. Mol Cell Biol. 2004; 24:5340–5352. [PubMed: 15169898]
25. Samayawardhena LA, Kapur R, Craig AW. Involvement of Fyn kinase in Kit and integrin-mediated Rac activation, cytoskeletal reorganization, and chemotaxis of mast cells. Blood. 2007; 109:3679–3686. [PubMed: 17213284]

26. Tan BL, Yazicioglu MN, Ingram D, McCarthy J, Borneo J, Williams DA, Kapur R. Genetic evidence for convergence of c-Kit- and α_4 integrin-mediated signals on class IA PI-3kinase and the Rac pathway in regulating integrin-directed migration in mast cells. Blood. 2003; 101:4725–4732. [PubMed: 12560232]
27. Gilfillan AM, Rivera J. The tyrosine kinase network regulating mast cell activation. Immunol Rev. 2009; 228:149–169. [PubMed: 19290926]
28. Yu M, Luo J, Yang W, Wang Y, Mizuki M, Kanakura Y, Besmer P, Neel BG, Gu H. The scaffolding adapter Gab2, via Shp-2, regulates kit-evoked mast cell proliferation by activating the Rac/JNK pathway. J Biol Chem. 2006; 281:28615–28626. [PubMed: 16873377]
29. O'Laughlin-Bunner B, Radosevic N, Taylor ML, Shivakrupa C, DeBerry C, Metcalfe DD, Zhou M, Lowell C, Linnekin D. Lyn is required for normal stem cell factor-induced proliferation and chemotaxis of primary hematopoietic cells. Blood. 2001; 98:343–350. [PubMed: 11435302]
30. Samayawardhena LA, Pallen CJ. Protein-tyrosine phosphatase α regulates stem cell factor-dependent c-Kit activation and migration of mast cells. J Biol Chem. 2008; 283:29175–29185. [PubMed: 18725415]
31. Dance M, Montagner A, Salles JP, Yart A, Raynal P. The molecular functions of Shp2 in the Ras/mitogen-activated protein kinase (ERK1/2) pathway. Cell Signal. 2008; 20:453–459. [PubMed: 17993263]
32. Futami M, Zhu QS, Whichard ZL, Xia L, Ke Y, Neel BG, Feng GS, Corey SJ. G-CSF receptor activation of the Src kinase Lyn is mediated by Gab2 recruitment of the Shp2 phosphatase. Blood. 2011; 118:1077–1086. [PubMed: 21636860]
33. Yu L, Min W, He Y, Qin L, Zhang H, Bennett AM, Chen H. JAK2 and SHP2 reciprocally regulate tyrosine phosphorylation and stability of proapoptotic protein ASK1. J Biol Chem. 2009; 284:13481–13488. [PubMed: 19287004]
34. Alai M, Mui AL, Cutler RL, Bustelo XR, Barbacid M, Krystal G. Steel factor stimulates the tyrosine phosphorylation of the proto-oncogene product, p95vav, in human hemopoietic cells. J Biol Chem. 1992; 267:18021–18025. [PubMed: 1381360]
35. Matsuguchi T, Inhorn RC, Carlesso N, Xu G, Druker B, Griffin JD. Tyrosine phosphorylation of p95Vav in myeloid cells is regulated by GM-CSF, IL-3 and steel factor and is constitutively increased by p210BCR/ABL. EMBO J. 1995; 14:257–265. [PubMed: 7530656]
36. del Pozo MA, Price LS, Alderson NB, Ren XD, Schwartz MA. Adhesion to the extracellular matrix regulates the coupling of the small GTPase Rac to its effector PAK. EMBO J. 2000; 19:2008–2014. [PubMed: 10790367]
37. Charest PG, Firtel RA. Feedback signaling controls leading-edge formation during chemotaxis. Curr Opin Genet Dev. 2006; 16:339–347. [PubMed: 16806895]
38. McDaniel AS, Allen JD, Park SJ, Jaffer ZM, Michels EG, Burgin SJ, Chen S, Bessler WK, Hofmann C, Ingram DA, et al. Pak1 regulates multiple c-Kit mediated Ras-MAPK gain-in-function phenotypes in $Nf1^{+/-}$ mast cells. Blood. 2008; 112:4646–4654. [PubMed: 18768391]
39. Zhang X, He Y, Liu S, Yu Z, Jiang ZX, Yang Z, Dong Y, Nabinger SC, Wu L, Gunawan AM, et al. Salicylic acid based small molecule inhibitor for the oncogenic Src homology-2 domain containing protein tyrosine phosphatase-2 (SHP2). J Med Chem. 2010; 53:2482–2493. [PubMed: 20170098]
40. Yang FC, Kapur R, King AJ, Tao W, Kim C, Borneo J, Breese R, Marshall M, Dinauer MC, Williams DA. Rac2 stimulates Akt activation affecting BAD/Bcl-XL expression while mediating survival and actin function in primary mast cells. Immunity. 2000; 12:557–568. [PubMed: 10843388]
41. Zhang SQ, Yang W, Kontaridis MI, Bivona TG, Wen G, Araki T, Luo J, Thompson JA, Schraven BL, Philips MR, Neel BG. Shp2 regulates SRC family kinase activity and Ras/Erk activation by controlling Csk recruitment. Mol Cell. 2004; 13:341–355. [PubMed: 14967142]
42. Kai M, Yasuda S, Imai S, Kanoh H, Sakane F. Tyrosine phosphorylation of β2-chimaerin by Src-family kinase negatively regulates its Rac-specific GAP activity. Biochim Biophys Acta. 2007; 1773:1407–1415. [PubMed: 17560670]

43. Wertheimer E, Gutierrez-Uzquiza A, Rosemblit C, Lopez-Haber C, Sosa MS, Kazanietz MG. Rac signaling in breast cancer: a tale of GEFs and GAPs. Cell Signal. 2012; 24:353–362. [PubMed: 21893191]

44. Stewart RA, Sanda T, Widlund HR, Zhu S, Swanson KD, Hurley AD, Bentires-Alj M, Fisher DE, Kontaridis MI, Look AT, Neel BG. Phosphatase-dependent and -independent functions of Shp2 in neural crest cells underlie LEOPARD syndrome pathogenesis. Dev Cell. 2010; 18:750–762. [PubMed: 20493809]

45. Yu ZH, Xu J, Walls CD, Chen L, Zhang S, Zhang R, Wu L, Wang L, Liu S, Zhang ZY. Structural and mechanistic insights into LEOPARD syndrome-associated SHP2 mutations. J Biol Chem. 2013; 288:10472–10482. [PubMed: 23457302]

46. Mali RS, Ma P, Zeng LF, Martin H, Ramdas B, He Y, Sims E, Nabinger S, Ghosh J, Sharma N, et al. Role of SHP2 phosphatase in KIT-induced transformation: identification of SHP2 as a druggable target in diseases involving oncogenic KIT. Blood. 2012; 120:2669–2678. [PubMed: 22806893]

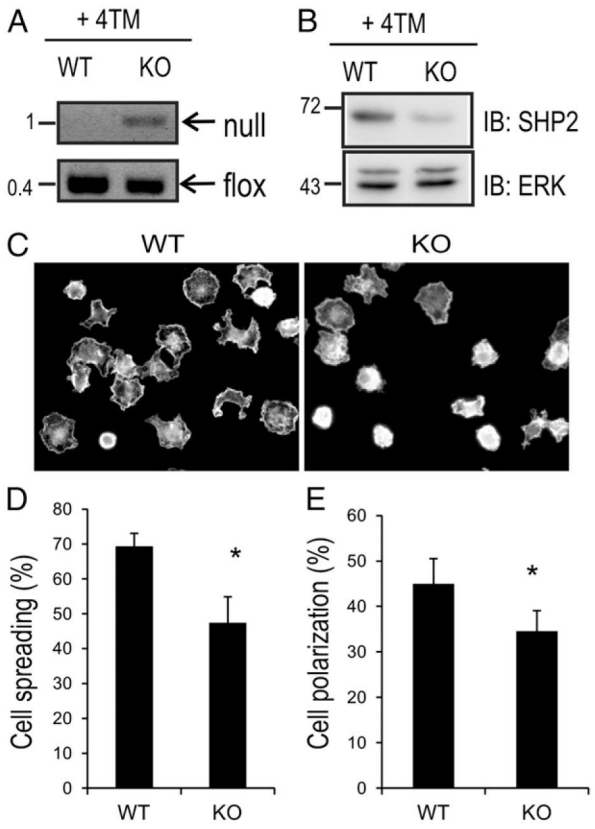

FIGURE 1.

Defective cell spreading and polarization in SHP2 KO BMMCs treated with SCF. (**A**) BMMCs obtained from $Shp2^{fl/fl}$ and Tg^{CreER}:$Shp2^{fl/fl}$ were treated with 4-TM (200 nM) for 3 d to generate WT and KO BMMCs, respectively. (A) PCR analyses of Shp2 null and flox alleles for genomic DNA isolated from WT and KO BMMCs. Position of DNA size markers (kilobases) are shown on the *left*. (**B**) IB analysis for WT and KO BMMC lysates probed with SHP2 and ERK Abs. Positions of relative mass markers (kDa) are shown on the *left*. (**C**) WT and KO BMMCs were straved of IL-3 for 6 h and seeded on fibronectin-coated coverslips in the presence of SCF (25 ng/ml for 45 min). Cells were fixed, permeabilized, and stained with TRITC–phalloidin. Representative epiflourescence micrographs are shown for F-actin staining. (**D**) The graph depicts the percentage of cells that had spread for multiple fields for WT and KO BMMCs ($n = 4 > 200$ cells; mean ± SD; triplicate samples; $*p < 0.05$, significant difference between genotypes. (**E**) Graph depicts the percentage of cells that had polarized for multiple fields for WT and KO BMMCs ($n = 4$, >200 cells; mean ± SD; triplicate samples; $*p < 0.05$, significant difference between genotypes.

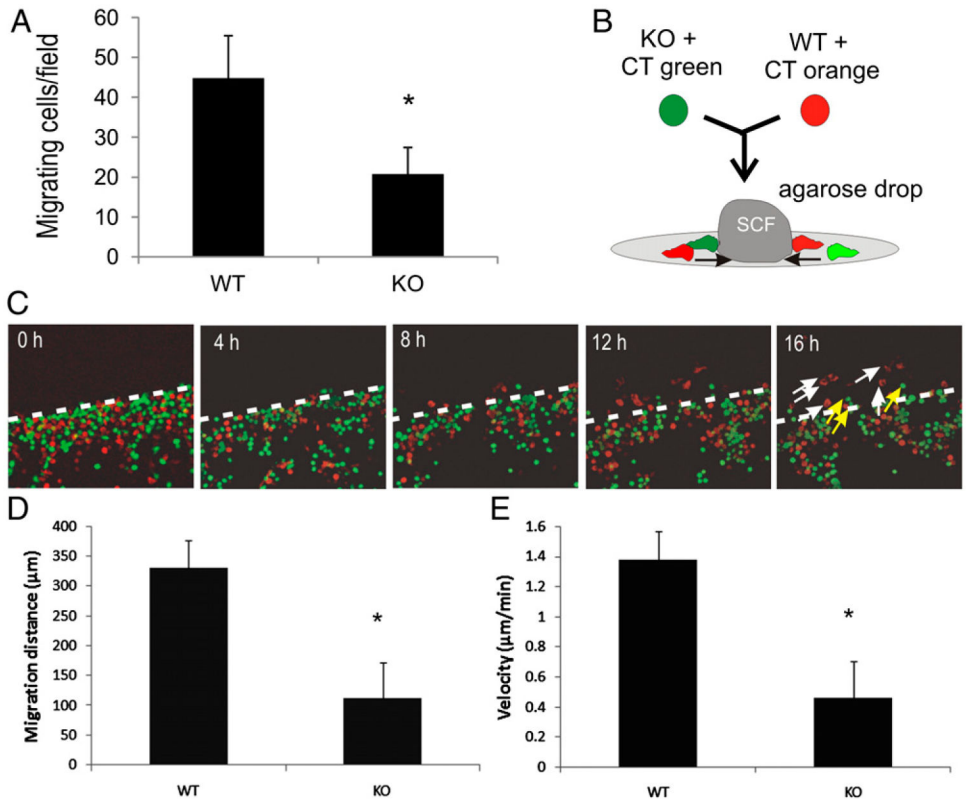

FIGURE 2.

SHP2 promotes chemotaxis of BMMCs. (**A**) Transwell assays were performed to measure WT and KO BMMC chemotaxis toward SCF (25 ng/ml). The graph depicts the number of cells per field (mean ± SD, $n = 3$ replicates, triplicate samples; $*p < 0.05$, significant difference between genotypes). (**B**) Schematic representation of experimental design using live cell imaging of agarose drop assays. WT and KO BMMCs were stained with CellTracker Orange and Green, respectively, and mixed prior to subjecting to SCF-embedded agarose drop chemotaxis assay, as described in *Materials and Methods*. (**C**) Representative confocal micrographs showing the positions of WT and KO BMMCs at the indicated times (0–16 h) during the time lapse are shown (margin of agarose drop indicated by dashed white line). White and yellow arrows depict positions of WT and KO BMMCs, respectively, that had migrated under the agarose at 16 h. (**D**) Cells from multiple fields ($n = 5$, >30 cells/genotype) were tracked individually to calculate migration distances (micrometers). The graph depicts mean migration distance (± SD) for WT and KO BMMCs ($*p < 0.05$, significant difference between genotypes). (**E**) Graph depicts the average velocity (micrometer per minute) for the same set of WT and KO BMMCs described in (D) ($*p < 0.05$, significant difference between genotypes).

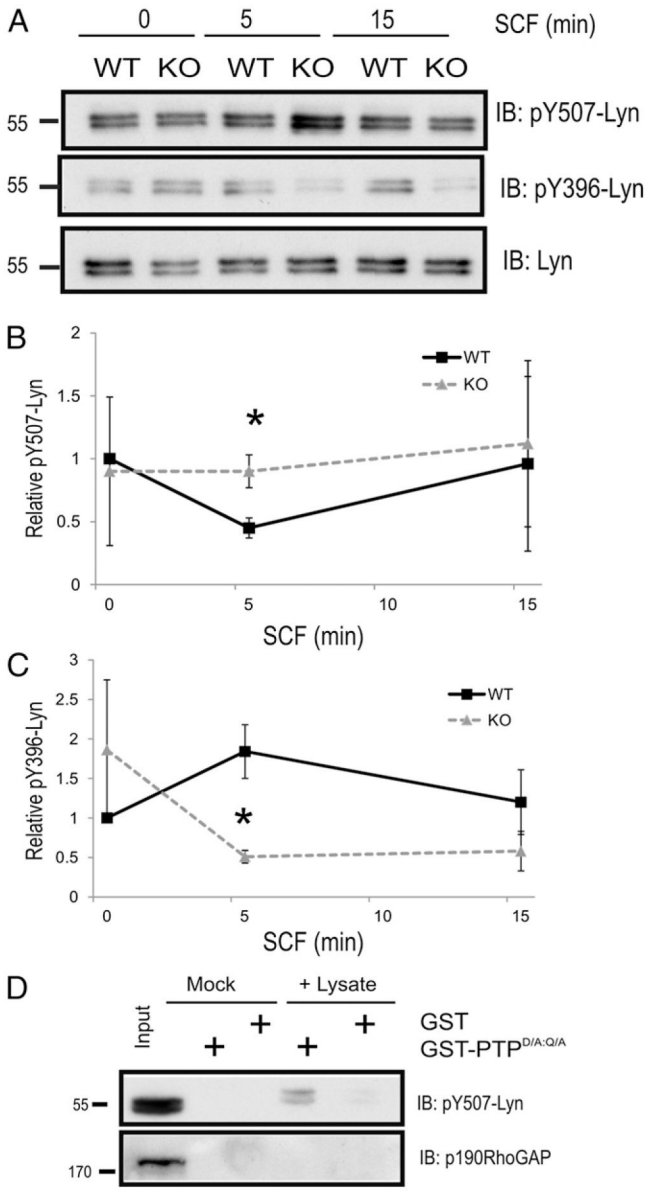

FIGURE 3.

Lyn C-terminal inhibitory tyrosine residue (pY507) is a direct substrate of SHP2. (**A**) WT and KO BMMCs were starved of IL-3 for 6 h and stimulated with SCF (50 ng/ml) for indicated times. Lysates were subjected to IB analysis with pY507-Lyn, pYSrc 416 (cross-reacts with pY396 Lyn) and Lyn Abs. (**B** and **C**) Line graph depicting the relative phosphotyrosine levels of Lyn at tyrosines 507 and 396, respectively, at indicated time points (mean ± SD; $n = 3$; $*p < 0.05$, significant difference between genotypes). (**D**) Lysates were prepared from SCF-treated Baf/3-KIT SHP2 KD cells (50 ng/ml for 5 min) and incubated with either GST or GST-PTP$^{D/A:Q/A}$ bound to beads overnight at 4°C. Mock reactions were performed with including lysates. IB analyses were carried out with Abs indicated on the *right*.

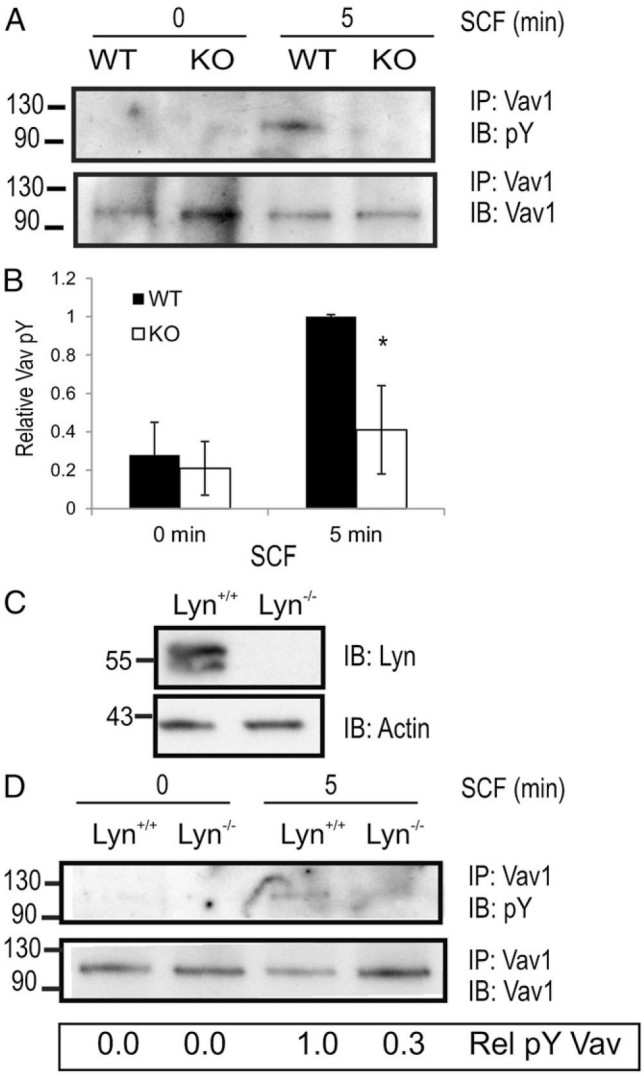

FIGURE 4.

SHP2 and Lyn promote phosphorylation of Vav1 downstream of KIT. (**A**) Lysates prepared from WT and KO BMMCs were subjected to IP with anti-Vav1 prior to IB analysis using anti-pY (PY99) and anti-Vav1. Positions of relative mass markers (kilodaltons) are shown on the *left*. (**B**) Graph depicting the relative total phosphotyrosine levels of Vav1 at indicated time points (mean ± SD; $n = 4$; $*p < 0.05$, significant difference between genotypes). (**C**) Lysates prepared from $Lyn^{+/+}$ and $Lyn^{-/-}$ BMMCs were subjected to IB analysis with anti-Lyn and anti-actin. (**D**) Lysates prepared from $Lyn^{+/+}$ and $Lyn^{-/-}$ BMMCs were subjected IP with anti-Vav1 prior to IB analysis using anti-pY (PY99) and anti-Vav1. Positions of relative mass markers (kilodaltons) are shown on the *left*.

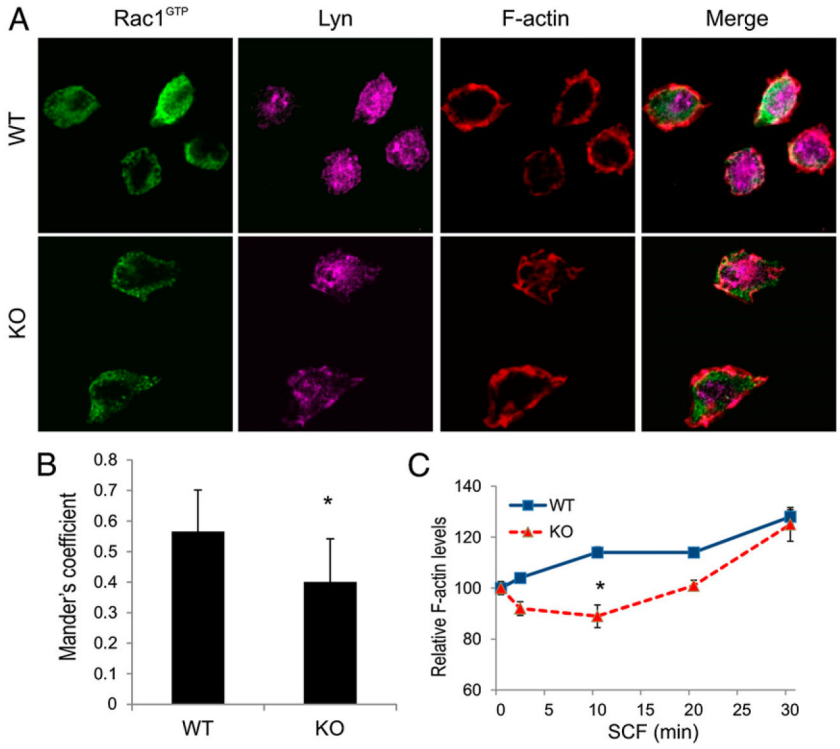

FIGURE 5.

Reduced plasma membrane Rac^{GTP} and F-actin polymerization in SHP2 KO BMMCs treated with SCF. (**A**) WT and KO BMMCs were starved of IL-3 for 6 h and plated on fibronectin-coated coverslips in presence of SCF (25 ng/ml for 45 min). Fixed and permeabilized cells were subjected to immunofluorescence staining with anti-active Rac1 ($Rac1^{GTP}$ conformation specific) and anti-Lyn. The TIRF micrograph depicting the ventral surface of the cells staining membrane fraction of active Rac1 and Lyn and the merge image of active Rac1 and Lyn channel. (**B**) Graph depicting the quantification analysis Mander's coefficient to measure the degree of colocalization of active Rac1 and Lyn channels between WT and KO genotypes. (mean ± SD; $n = 20$; $*p < 0.05$, significant difference between genotypes). (**C**) Cytokine starved WT and KO BMMCs were stimulated with SCF (100 ng/ml) for indicated times, fixed, and permeablized prior to staining with Alexa Fluor 488–conjugated phalloidin. The graph depicts the percentage change in F-actin mean fluorescence intensity (mean ± SD; triplicate samples) for WT and KO BMMCs compared with 0 min ($*p < 0.05$, significant difference between genotypes).

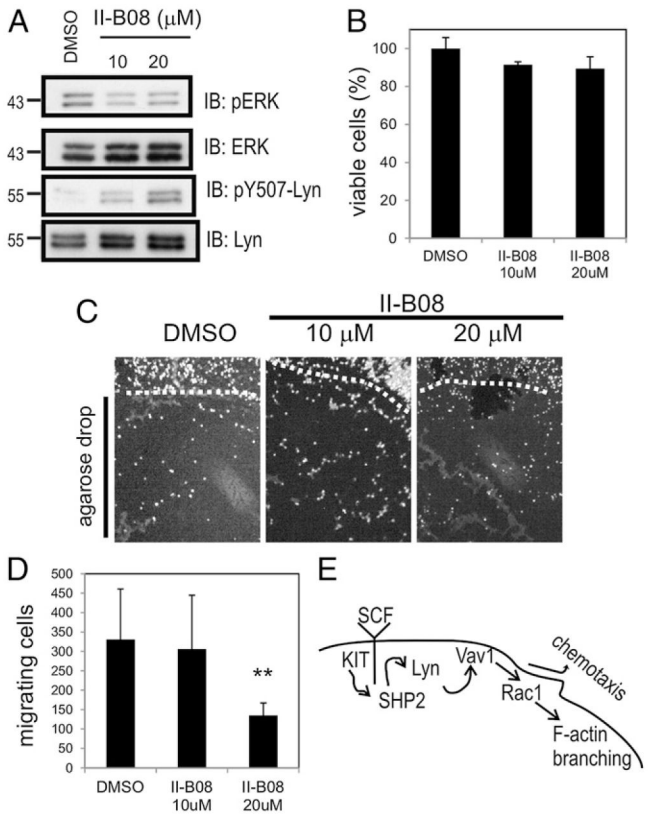

FIGURE 6.

SHP2 phosphatase activity promotes chemotaxis of BMMCs toward SCF. (**A**) BMMCs grown in IL-3 and SCF for 3 wk were pretreated with vehicle (DMSO) or different concentrations of SHP2 inhibitor (II-B08; 10 or 20 μM) for 1 h. Lysates were subjected to IB analysis with anti-pERK, anti–phospho-Lyn (pY507), ERK, and Lyn Abs. (**B**) BMMCs grown in IL-3 and SCF for 3 wk were pretreated with DMSO or different concentrations of II-B08 as above for 24 h. The graph depicting the percent cell viability determined with alamar blue assay as described in *Materials and Methods* (mean ± SD; triplicate samples). (**C**) Cytokine-starved BMMCs were pretreated for 1 h and maintained with either vehicle (DMSO) or different concentrations of SHP2 inhibitor (II-B08; 10 or 20 μM) prior to plating on fibronectin-coated coverslips containing SCF-embedded agarose drops. After 18 h, cells were fixed and stained with DAPI, and the images were acquired on an epifluorescence microscope. Representative micrographs are shown for $DAPI^+$ cells at the margin of the agarose drop (dashed line) and underneath the agarose drop (below the dashed line). (**D**) The graph depicting the total number of BMMCs that had migrated under each SCF-embedded agarose drop ($n = 3$ replicates, triplicate samples; $^{**}p < 0.01$, statistical significant difference between the genotype). (**E**) Simplified pathway model relating SHP2 to mast cell chemotaxis. SHP2 promotes Lyn activation downstream of KIT, leading to Vav1 phosphorylation, Rac activation, and F-actin branching and polymerization required for chemotaxis.